A. Ozgurluk and C. T.-C. Nguyen, "Precision residual strain sensor employing gap-dependent frequency shift," *Proceedings*, IEEE Joint Conf. of the IEEE Int. Frequency Contr. Symp. & IEEE Int. Symp. on Applications of Ferroelectrics, Virtual Conference, July 19-23, 2020, DOI: 10.1109/IFCS-ISAF41089.2020.9234911.

Precision Resonant Beam Strain Sensor Employing Gap-Dependent Frequency Shift

Alper Ozgurluk and Clark T.-C. Nguyen

Berkeley Sensor & Actuator Center (BSAC)
Dept. of Electrical Engineering and Computer Sciences
University of California at Berkeley
Berkeley, California, USA
ozgurluk@eecs.berkeley.edu

***Abstract*—A micromechanical structure for on-chip strain sensing maps strain-induced gap changes to resonance frequency shifts while employing differential strategies to null out bias uncertainty, all towards repeatable measurement of sub-nm displacement changes that equate to sub-με strain increments. The key enabler here is the use of gap-dependent electrical stiffness to shift resonance frequencies as structural elements stretch or shrink to relieve stress. An output based on the difference frequency between two close proximity structures with unequal stress arm lengths (*cf.* Fig. 1) removes uncertainty on the initial gap spacing and permits a 206 Hz/με scale factor. The ability to precisely measure the frequency of the high-*Q* (~4000) structures, down to at least 1 Hz, puts the resolution of this sensor at least 5 nε (or 790 Pa for polysilicon). An on-chip highly sensitive strain sensing device like this will likely be instrumental to managing stress changes over the lifetime of micromechanical circuits, such as oscillators and filters.**

***Keywords*—MEMS, micromechanical resonator, polysilicon, strain, stress, diagnostic, electrical stiffness**

I. Introduction

Recently demonstrated sub-20-nm capacitive-gap transduced resonators with C_x/C_o's of 71% at 10-MHz [1] and 1% at 200-MHz [2] now introduce compelling combinations of high Q and strong electromechanical coupling at HF and VHF [3] [2] that could change the landscape of applications available to MEMS. However, small electrode-to-resonator gaps also make more difficult the design and realization of MEMS-based mechanical circuits, e.g., filters and oscillator arrays [4], that become more prone to post-fabrication residual stress [5] as circuit size and gap spacing increase and decrease, respectively. Although recent design [5] and fabrication [6] strategies have greatly improved yields, a strain sensor able to precisely measure strain in close proximity to a device would permit real-time correction for strain-induced shifts, e.g., from package stress deviations, as well as optimization of the process recipes used to fabricate small-gap devices.

To this point, existing on-chip stress/strain sensors in the literature either use very specific material systems that limit their applicability, or if widely applicable, are not sufficiently sensitive. For example, the high resolution on-chip strain sensor of [7] relies on piezoelectric material, which is often not compatible with surface-micromachining fabrication processes

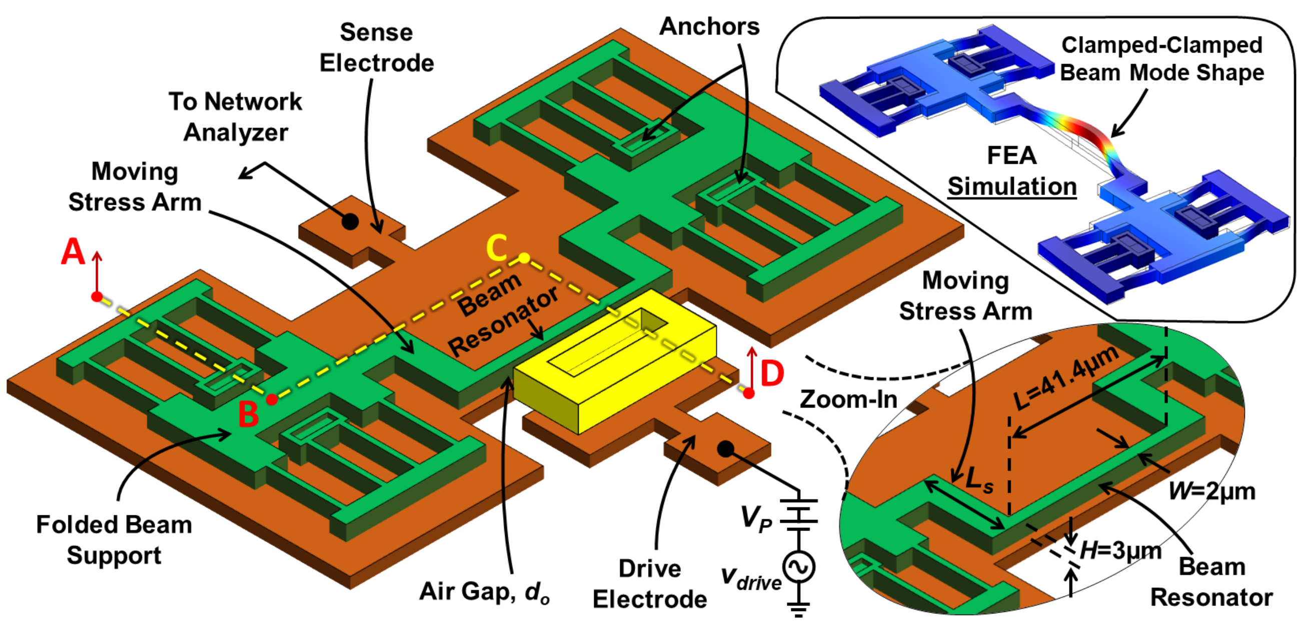

Fig. 1: The on-chip beam resonator strain sensor described herein in a typical operating circuit along with the key dimensions. The inset shows the finite element analysis (FEA) simulated mode shape during strain determination.

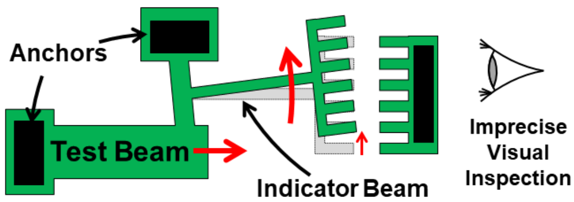

Fig. 2: Previous on-chip vernier stress gauge of [11].

used to achieve MEMS devices made in conductive materials, e.g., doped polysilicon or metal. This reduces the range of MEMS devices for which they can serve as on-chip strain sensors.

On the other hand, on-chip strain sensors available via surface-micromachining often lack sufficient resolution [8], [9], [10]. For example, the surface-micromachined Vernier stress gauge depicted in Fig. 2 [11] employs visual determination of indicator beam movement under a microscope—a procedure that clearly lacks precision. This structure also is most sensitive when its indicator beam is long, since this amplifies its movement under a given strain. The need for long length, however, renders the device vulnerable to vertical stress gradients, placing a limit on the minimum measurable stress.

The quest for on-chip strain sensing with high resolution calls for a sensor with a more precise readout method, e.g., frequency, that better decouples strain resolution from structure size. The sensor described herein and summarized in Fig. 1 does precisely this via use of a micromechanical structure that maps strain-induced gap changes to resonance frequency shifts while employing differential strategies to null out bias uncertainty, all towards repeatable measurement of sub-nm displacement changes that equate to sub-με increments. The next section describes in more detail the basic operation principle.

II. Electrical Stiffness-Based Strain Sensor

The strain sensor of Fig. 1 comprises a conductive polysilicon beam resonator suspended by crab legs to folded-beam anchoring structures designed to relieve stress along the beam's axis, as indicated by the finite-element simulations of Fig. 3. The stress relief is instrumental to preventing beam buckling that might otherwise short the beam to an overlapping side doped polysilicon electrode spaced only 60 nm away. This small gap spacing determines not only the strength of the capacitive-gap transducer used to drive the beam into resonance vibration and sense said vibration, but also the magnitude of the electrical stiffness between the beam and electrode.

The key enabler in the subject strain sensor is the use of a gap-dependent electrical stiffness to shift the resonance frequency as structural elements stretch, shrink, or otherwise move relative to one another with applied stress. The Fig. 1 strain sensor specifically uses this shift in frequency to measure the nm-level change in gap spacing d_o between the structure and a capacitive-gap transducing electrode. The gap change then indicates the strain. Perhaps the best vehicle with which to describe sensor operation is during measurement of the post-fabrication residual stress often generated via thermal expansion differences between the substrate and the suspended materials.

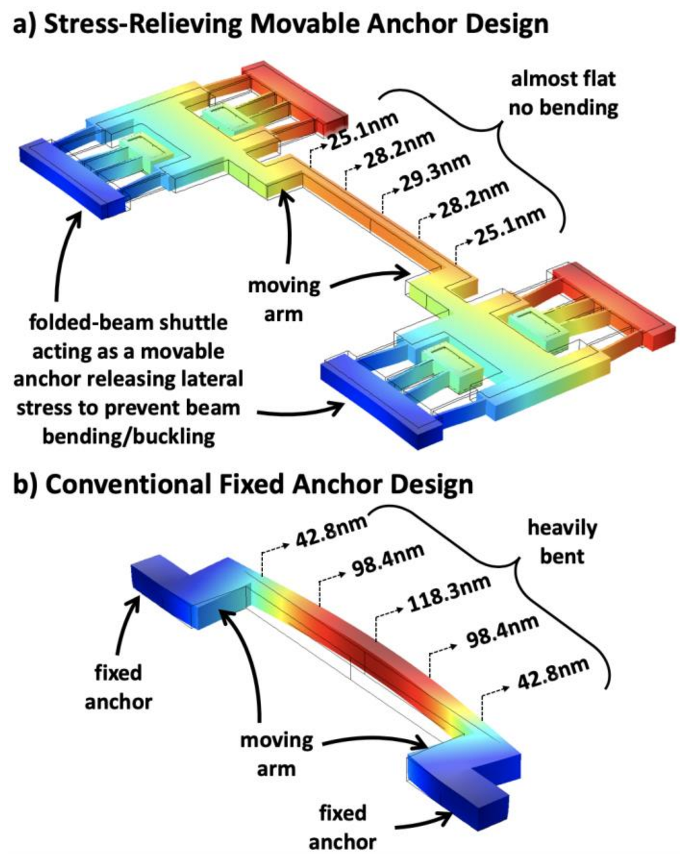

Fig. 3: Stationary FEA simulations under 500 MPa residual stress for polysilicon structural layer with a) lateral stress-relieving movable anchor design b) conventional fixed anchor design. The simulation results clearly show the stress-relieving design successfully avoids beam bending and enables more uniform gap reduction under compressive stress.

A. Post-Fabrication Residual Stress Measurement

Measurement of residual stress using the device of Fig. 1 amounts to measuring the nm-level expansion/contraction of a movable stress arm of length L_s as a change in capacitive transduction gap d_o. Here, before release, the structure is under compressive stress due to thermal expansion differences between the substrate and structural layer, as depicted in Fig. 4(a). After removing the sacrificial spacer as shown in Fig. 4(b), the stress arm L_s relieves compressive stress by stretching a few nanometers, thereby shrinking the gap in proportion to its length, i.e., a longer arm leads to a larger reduction in the gap, according to

$$\Delta d_o = -\varepsilon L_s \tag{1}$$

where Δd_o is the strain-based gap change after release and ε is the residual strain. If the gap also serves in a capacitive-gap transducer for the indicated beam, the reduction in gap spacing induces an increase in electrical stiffness k_e according to [12]

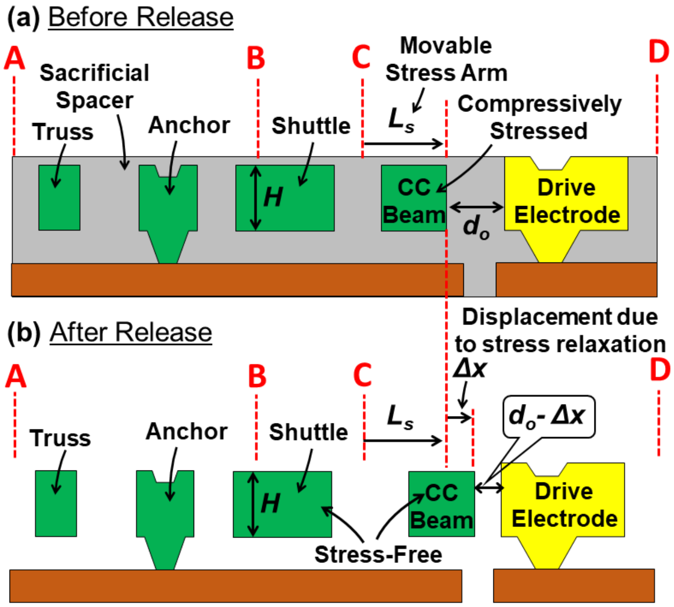

Fig. 4: Cross-sections through ABCD (a) before release (b) after release.

$$k_e = \frac{\varepsilon_o H L_e V_P^2}{(d_o - \Delta d_o)^3} \approx \frac{\varepsilon_o H L_e V_P^2}{d_o^3}\left(1 + \frac{3\Delta d_o}{d_o}\right) \tag{2}$$

where ε_o is the free-space permittivity, H is the beam thickness, L_e is the electrode length, and V_P is the dc-bias voltage, and the last form assumes the change in gap spacing Δd_o is much smaller than the initial gap d_o. This change in electrical stiffness in turn reduces the beam's resonance frequency to

$$f_o = f_{nom}\sqrt{1 - k_e/k_m} \approx f_{nom}\left(1 - \frac{k_e}{2k_m}\right) \tag{3}$$

where f_{nom} is the beam's nominal purely mechanical resonance frequency [13]

$$f_{nom} = 1.03\frac{W}{L^2}\sqrt{E/\rho} \tag{4}$$

where W is the beam width, L is the beam length, E and ρ are the Young's modulus and density, respectively, and k_m is the mechanical stiffness

$$k_m = 4\alpha\pi^2 f_{nom}^2 \rho WHL \tag{5}$$

where α is a constant relating the actual beam mass to the equivalent mass [14]. Assuming the electrical stiffness is much smaller than the mechanical stiffness and substituting (1), (2) and (5) in (3), the frequency change Δf_s, which is precisely measurable, then gauges the strain according to

$$\varepsilon = \frac{d_o}{3L_s}\left(1 - \frac{8\alpha\pi^2\rho WLf_{nom}d_o^3}{\varepsilon_o L_e V_P^2}\Delta f_s\right) \tag{6}$$

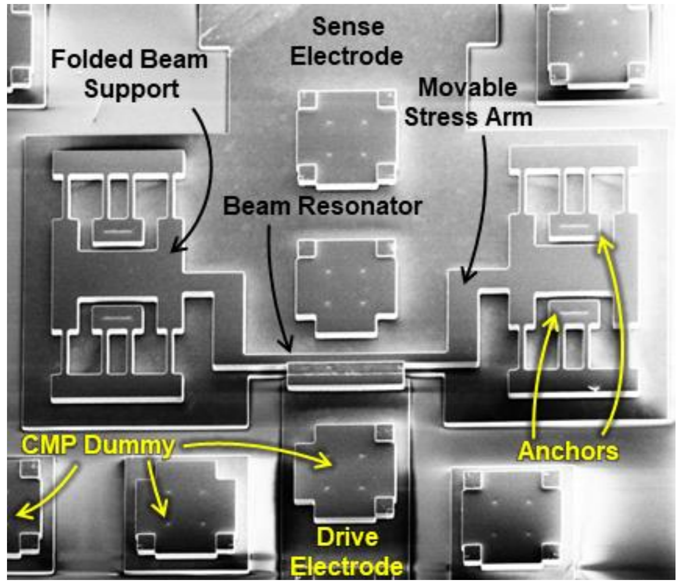

Fig. 5: SEM of a fabricated polysilicon strain diagnostic device.

where $\Delta f_s = f_{nom} - f_o$. An opposite change in gap, i.e., an increase, would indicate tensile stress.

The strong dependence of (6) on gap spacing d_o puts a premium on suppressing phenomena other than the strain along the sense axis that might also influence the gap spacing. One such phenomena is stress along the beam axis, which is orthogonal to the sense direction, but can buckle the resonator beam and thereby change the gap. This underscores the utility of the previously mentioned folded-beam anchors at the ends of the resonant sensing beam that suppress axial stress, as shown in Fig. 3.

B. *General Stress Measurement*

Knowledge of fabrication residual strain via (6) then permits isolation of strain due other causes, i.e., the external strain, e.g., package stress, by merely subtracting out the gap change due to residual strain from the total gap change. Here, the remaining gap amount corresponds to the external strain.

III. Measurement Results

Fig. 5 presents an SEM of the residual strain sensor fabricated alongside tiny-gap mechanical filters, i.e., in the same surface-micromachining process [5]. The fabrication run included several designs like this with 41.3-µm-long, 2-µm-wide, 3-µm-thick resonant beams and various stress arm lengths.

Fig. 6 presents frequency spectra measured under 50-µTorr vacuum over a dc-bias V_P range from 1 V to 5 V for two structures fabricated side by side that are identical in all respects except for different support arm lengths (L_s's) of 10 µm and 20 µm. The different lengths lead to final gaps extracted by curve-fitting the measurement data [12] of 52.4 nm and 45.7 nm, respectively. Assuming the starting gap for each is 60 nm, these correspond to -760 and -715 µstrain, respectively, using (1).

Note that the accuracy of resulting strain depends on knowledge of the initial gap d_o. Unfortunately, fabrication

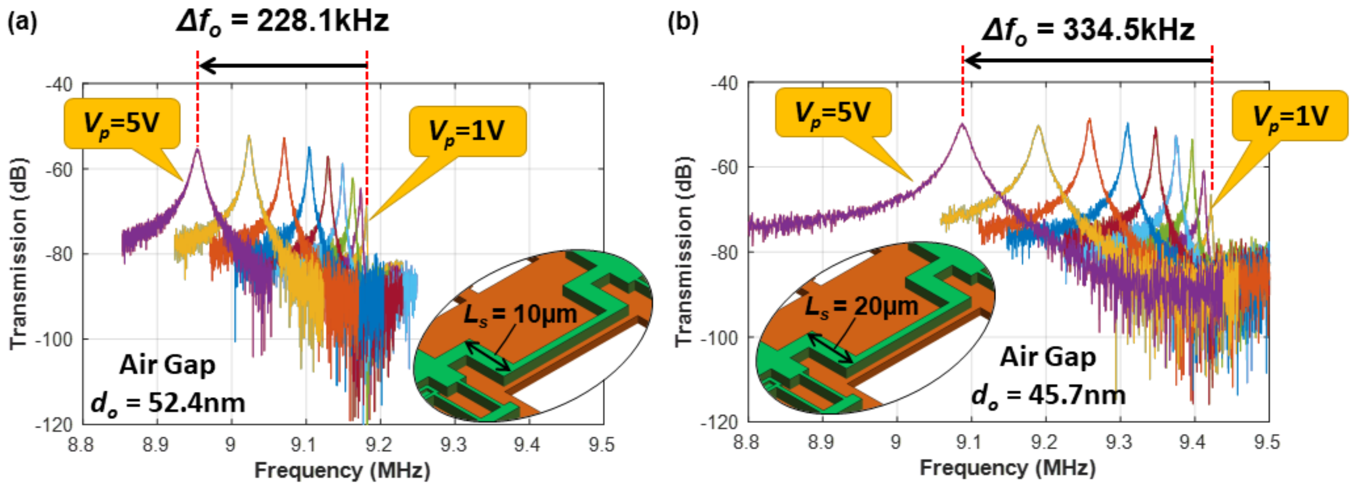

Fig. 6: Measured frequency spectra under 50-µTorr vacuum for polysilicon beam resonant strain sensors as a function of dc-bias voltage using (a) short (L_s = 10µm) and (b) long (L_s = 20µm) moving stress arm. Each sensor used identical resonant beams 41.8-µm long, 2-µm wide, and 3-µm thick.

tolerances and statistical deviations make it difficult to know d_o accurately. (Thus, the need to assume a d_o in the previous strain determinations.) To address this problem, a differential approach is possible if two close-proximity sensors with different stress arm lengths are available. Specifically, a strain value independent of the initial gap results from taking the difference between extracted gaps for the 10-µm and 20-µm stress arm length cases and dividing this by the difference in stress arm lengths:

$$\varepsilon = \frac{d_{o2} - d_{o1}}{L_{s2} - L_{s1}} = \frac{45.7 - 52.4}{20 - 10} \times \frac{10^{-9}}{10^{-6}} = -670\ \mu\varepsilon \qquad (7)$$

where d_{o1} and d_{o2} are the gaps for the 10-µm and 20-µm stress arm sensors, respectively. This now is a more accurate value of stress.

A. Faster Methods

Curve-fitting is perhaps the most accurate method to extract the final gap and hence the strain. It does, however, require collection of numerous data points to attain an accurate answer. While the procedure for doing this can be automated in a way that provides outputs fast enough for stress compensation, e.g., for an oscillator, (6) provides a simpler, faster method. However, (6) also requires knowledge of the initial gap spacing d_o and the unbiased nominal resonance frequency f_{nom}. While the latter might be obtained by extrapolating a resonance frequency f_o vs. dc-bias V_P curve to zero dc-bias, this still requires collection of numerous points, after which the extracted f_{nom} can be used in all future calculations using (6). But this need only be done once.

Using (6) with an (assumed) initial gap d_o of 60 nm, α of 0.3965, ρ of 2300 kg/m^3, E of 158 GPa, W of 2 µm, L of 41.3 µm, L_e of 24 µm, V_p of 5 V, Δf_{s1} of 228.1 kHz, and Δf_{s2} of 334.5 kHz, the strains for the 10-µm and 20-µm stress arm cases are -895 and -190 µstrain, respectively. Of the two of these, the former for the 10-µm-long stress arm is more correct, since it derives from a smaller percent gap change. Indeed, the amount of gap change for the 20-µm case is a significant fraction of the initial gap, making (2) and hence (6) much less accurate.

If two strain sensors with differing stress beams have the same f_{nom}, then the need to know f_{nom} goes away via use of the difference in strain-derived frequency shifts between the two structures. In this case, the specific expression for strain becomes

$$\varepsilon = -8.24\frac{\alpha\pi^2 W^2\sqrt{E\rho}\,d_o^4}{3\varepsilon_o L_e V_P^2 L}\left(\frac{\Delta f_{s2} - \Delta f_{s1}}{L_{s2} - L_{s1}}\right) \qquad (8)$$

where L_{s1} and L_{s2} are the support arm lengths and Δf_{s1} and Δf_{s2} are the frequency shifts for the two designs, respectively. This expression still contains the initial gap spacing d_o, so still contains some uncertainty, but its impact on (8) is smaller than on (6). Here, using a single nominal d_o in the numerator yields a more intuitive closed-form expression.

Since the nominal resonance frequencies of the two sensors herein are not quite the same, use of (8) is not particularly advantageous, here. Nevertheless, using (8) with data from Fig. 6(a) and (b) and the target d_o of 60 nm yields -515.3 µstrain, which interestingly is not far from the -670 µstrain of (7).

B. Scale Factor (Sensitivity)

Scale factor or sensitivity of a resonant sensor indicates how much its frequency shifts in response to a change in strain. Employing this definition by taking the partial derivative of (8) with respect to strain yields

$$\frac{\partial \Delta f}{\partial \varepsilon} = -\frac{3\varepsilon_o L_e V_P^2 L(L_{s2} - L_{s1})}{8.24\alpha\pi^2 W^2\sqrt{E\rho}\,d_o^4} \qquad (9)$$

The inverse 4th power dependence on the actuation gap d_o generates extremely sensitive resonant sensing as gaps become smaller, i.e., sub-100nm. The 106.4-kHz difference in frequency excursions between Fig. 6 (a) and (b) over the measured 1V to 5V dc-bias voltage V_P range corresponds to

TABLE I. COMPARISON OF THIS WORK AND OTHER TECHNOLOGIES

Technology	**MEMS Cap.** [15]	**MEMS Piezo.** [7]	**MEMS Res.** [16]	**This Work**	**Unit**
Scale Factor	816μV	340μV	120Hz	206Hz	$\mu\varepsilon^{-1}$
Resolution	870	28.7	4	0.969	nε
Range	±1000	N/A	±2.5	±3000	με

81.4 MPa compressive stress. This puts the average scale factor at 206.5 Hz/με (1.31 Hz/kPa for polysilicon) over this range.

C. Resolution

Resolution, in the context of a resonant strain sensor, is the strain corresponding to the minimum detectable resonance frequency shift, which is usually limited by short-term frequency instability. Rearranging (8) and replacing Δf_{s2} - Δf_{s1} with $\sigma_{ymin} f_o$ where σ_{ymin} is the Allan deviation yields

$$\Delta\varepsilon = 8.24\frac{\alpha\pi^2 W^2\sqrt{E\rho}\,d_o^4\sigma_{ymin}}{3\varepsilon_o L_e V_P^2 L(L_{s2}-L_{s1})}f_o \tag{10}$$

Again, the 4th power dependence on the gap d_o implies a very high-resolution sensor with small gaps. Using a typical Allan deviation value of $2\text{x}10^{-8}$ at 1 s integration time measured for a wine-glass disk resonator fabricated in a similar process yields 0.969 nε resolution.

D. Range

Although there is technically no limit with high enough dc-bias voltages for measuring tensile strain, the actuation gap d_o ultimately limits the maximum measurable compressive strain as follows

$$\varepsilon_{max} = -d_o/L_{s2} \tag{11}$$

Here, a nominal actuation gap value of 60nm with a 20um-long support arm limits the compressive strain measurement range to ±3000 μstrain.

Table I summarizes the scale factor, resolution, and range for the strain sensor of this paper along with some other devices found in the literature.

IV. CONCLUSIONS

Given that the impressive sensitivity and resolution of the resonant strain sensors demonstrated herein derive from small electrode-to resonator gaps, recent technological advances that reduce gaps even further [2] will likely encourage many more sensors based on electrical stiffness changes. This is not to say that only small-gapped versions are of interest. Indeed, although this work targets small-gapped micromechanical circuits, it should be clear that this approach is applicable to larger gap devices, as well, since electrical stiffness is universal. Larger gap versions would likely use higher voltages and alternative geometries but could probably still achieve similarly impressive sensitivity and resolution.

V. ACKNOWLEDGMENT

The authors are grateful for funding support from the NSF and the Berkeley Sensor & Actuator Center.

VI. REFERENCES

[1] A. Ozgurluk, K. Peleaux and C. T.-C. Nguyen, "Widely tunable 20-nm-gap ruthenium metal square-plate resonator," in *Tech. Dig. 32nd IEEE Int. Conf. on Micro Electro Mechanical Systems (MEMS)*, Seoul, South Korea, 2019, pp. 153-156.

[2] A. Ozgurluk, K. Peleaux and C. T.-C. Nguyen, "Single-digit-nanometer capacitive-gap transduced micromechanical disk resonators," in *IEEE 33rd International Conference on Micro Electro Mechanical Systems (MEMS)*, Vancouver, Canada, 2020, pp. 222-225.

[3] G. Piazza, P. F. Stephanou and A. P. Pisano, "Piezoelectric Aluminum Nitride Vibrating Contour-Mode MEMS Resonators," *J. Microelectromechanical Syst.*, vol. 15, no. 6, pp. 1406-1418, 2006.

[4] Y.-W. Lin, S.-S. Li, Z. Ren and C. T.-C. Nguyen, "Low phase noise array-composite micromechanical wine-glass disk oscillator," in *Tech. Dig., IEEE Int. Electron Devices Mtg.*, Washington, D.C., 2005, pp. 287-290.

[5] M. Akgul, A. Ozgurluk and C. T.-C. Nguyen, "RF Channel-Select Micromechanical Disk Filters, Part II: Demonstration," *IEEE Trans. Ultrason., Ferroelect., Freq. Contr.*, vol. 66, no. 1, pp. 218-235, 2019.

[6] J. N. Nilchi, R. Liu and C. T.-C. Nguyen, "High Cx/Co 13nm-capacitive-gap transduced disk resonator," in *Tech. Dig. 30th IEEE Int. Conf. on Micro Electro Mechanical Systems (MEMS)*, Las Vegas, NV, 2017, pp. 924-927.

[7] S. Kon and R. Horowitz, "A high-resolution MEMS piezoelectric strain sensor for structural vibration detection," *IEEE Sensors J.*, vol. 8, no. 12, pp. 2027-2035, 2008.

[8] W. Fang and J. A. Wickert, "Post buckling of micromachined beams," *J. Micromech. Microeng.*, vol. 4, no. 3, pp. 116-122, 1994.

[9] J. Lu, Handbook of Measurement of Residual Stresses, Lulburn, GA: Fairmount Press, 1996.

[10] H. Guckel, D. Burns, C. Rutigliano, E. Lovell and B. Choi, "Diagnostic microstructures for the measurement of intrinsic strain in thin films," *J. Micromech. Microeng.*, vol. 2, no. 2, pp. 86-95, 1992.

[11] L. Lin, A. P. Pisano and R. T. Howe, "A micro strain gauge with mechanical amplifier," *J. Microelectromechanical Syst.*, vol. 6, no. 4, pp. 313-321, 1997.

[12] W.-T. Hsu and C. T.-C. Nguyen, "Stiffness-compensated temperature-insensitive micromechanical resonators," in *in Proc. IEEE International Conference Micro Electro Mechanical Systems (MEMS)*, Las Vegas, NV, 2002, pp. 731-734.

[13] A. Ozgurluk, R. Liu and C. T.-C. Nguyen, "Q-Boosting of Metal MEMS Resonators Via Localized Anneal-Induced Tensile Stress," in *Proc. Joint IEEE Int. Freq. Control Symp. Eur. Freq. Time Forum*, Besancon, France, 2017, pp. 10-15.

[14] F. D. Bannon III, J. R. Clark and C. T.-C. Nguyen, "High frequency micromechanical filters," *IEEE J. Solid-State Circuits*, vol. 35, no. 4, pp. 512-526, 2000.

[15] M. Suster, J. Guo, N. Chaimanonart, W. H. Ko and D. J. Young, "A Wireless Strain Sensing Microsystem with External RF Power Source and Two-Channel Data Telemetry Capability," in *IEEE Int. Solid State Circuits Conf.*, San Francisco, CA, 2007, pp. 380-609.

[16] L. Belsito, M. Ferri, F. Mancarella, A. Roncaglia, J. Yan, A. A. Seshia and K. Soga, "High-resolution strain sensing on steel by silicon-on-insulator flexural resonators fabricated with chip-level vacuum packaging," in *Proc. Int. Conf. Solid-State Sens., Actuators, Microsyst. Tech. Dig. (Transducers)*, Barcelona, Spain, 2013, pp. 992-995.